

An automated pipeline for photometric calibration and measurements

Alexi Mattila

aleksi.mattila@student oulu.fi

September 27, 2022

Abstract

Measuring magnitudes from astronomical images can be slow and difficult when done by hand, especially if there's a large amount of targets or images that need to be analysed. To aid in this effort, Autophotometer, an automatic pipeline for photometric measurements and calibrations was developed. Autophotometer was made with Python, and it uses Source Extractor and SCAMP from Astromatic. The photometric calibrations are performed using data from Pan-STARRS1 and 2MASS surveys.

This master's thesis describes the technical details of the pipeline and how it was used to study cataclysmic variables. Over 350 images of cataclysmic variables in multiple filters taken with the Nordic Optical Telescope were processed with the program to evaluate its performance and accuracy.

Most of the resulting magnitudes had errors comparable to those in Pan-STARRS1 and 2MASS catalogues. The accuracies were sufficient to analyse the spectral energy distributions of the targets and identify different types of cataclysmic variables. Some issues were encountered, mostly caused by bad image quality or very dim targets. In few cases the astrometric calibration of the coordinates of the objects failed. In general the program is reliable and easy to use.

Contents

1	Acknowledgements	5
2	Introduction	5
3	Photometry	7
3.1	Luminosity and Flux density	7
3.2	Magnitudes	7
3.3	Instrumental Magnitudes	9
3.3.1	Atmospheric Extinction	11
3.4	Photometric Systems and Surveys	13
3.4.1	Colour Corrections	14
3.4.2	Johnson-Cousins System	14
3.4.3	SDSS	15
3.4.4	Pan-STARRS1	16
3.4.5	2MASS	17
3.4.6	Transformations between systems	17
4	Program	19
4.1	Description	19
4.1.1	Supported Observatories and Filters	19
4.2	Installation	19
4.2.1	Requirements	19
4.2.2	Setup - Using pip	20
4.2.3	Setup - Manual	21
4.3	Usage	21
4.4	API Documentation	24
4.4.1	Coordinate correction	26

4.4.2	Cosmic ray removal	27
4.4.3	Star separation	27
4.4.4	Database access and coordinate matching.	28
4.4.5	Photometry calculations	29
4.4.6	Plotting	31
5	Practical use of the pipeline	32
5.1	Short scientific background	32
5.2	Process	33
5.3	Problems	41
5.3.1	Issues with data	41
5.3.2	Dense fields	41
5.3.3	Sparse fields	41
5.3.4	Locating targets	42
5.3.5	Effects of the colour term	44
5.4	Results and Discussion	44

1 Acknowledgements

This project was created using Python, and uses SExtractor (Bertin, E. and Arnouts, S., 1996) and SCAMP (Bertin, 2006) from Astromatic.

The Autophotometer program made use of Astropy,¹ a community-developed core Python package for Astronomy (The Astropy Collaboration et al., 2013, Price-Whelan et al., 2018). Additional packages used were Numpy (Harris et al., 2020), Matplotlib (Hunter, 2007), ccdproc (Craig et al., 2017), Photutils (Bradley et al., 2021), and Requests ².

2 Introduction

The measuring of the properties of starlight, or photometry, can be used to study the stars in great detail. It can be used to estimate the temperature or even the composition of a star. Some objects have variable brightness, which can be caused by many things. Some stars can pulsate, causing changes in their radius and temperature, and therefore varying their brightness and colour. Others can be eclipsing binaries or stars with exoplanets. These system's light curves show distinct features, as depicted in figure 1. The light curve can be used to estimate the periods and radii of the members of the system. If we have performed photometric measurements in different wavelengths, the spectral energy distributions of stars can also be studied, revealing more about the composition and properties of the system.

There are various methods of measuring the brightness of stellar objects. Doing it manually by hand can be slow, especially if one wishes to inspect a large number of stars. In this thesis is described a program that was created to per-

¹<http://www.astropy.org>

²<https://requests.readthedocs.io/en/latest/>

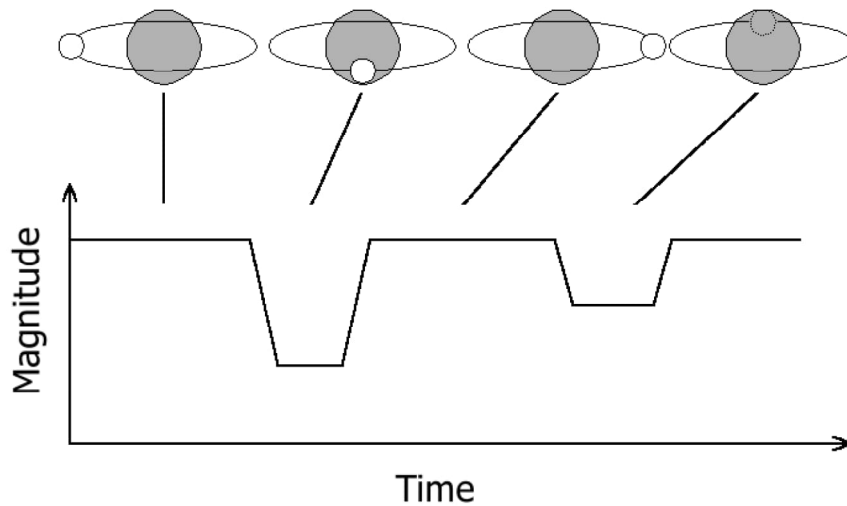


Figure 1: Illustration of the different phases of an eclipsing binary star system and its light curve.

form astrometric and photometric measurements faster and easier, and with good enough accuracy so the results can be used in research.

In the first part of the thesis some basics of concepts of photometry are explained. How the brightnesses of stars can be calculated, and what needs to be taken into account when measuring them. Then there are brief descriptions of the different photometric systems and surveys that are relevant in this study.

Next section contains the description of the Autophotometer program. There are instructions on how to install and use it. All the program's basic functionalities are described, along with what needs to be taken into account when using it.

The final section of the thesis describes the process of how Autophotometer was used to find magnitudes of a large number of objects. A number of issues emerged, but they could mostly be circumvented by adjusting the configuration parameters of the program.

3 Photometry

3.1 Luminosity and Flux density

The most important quantities regarding brightnesses of stars are luminosity L and flux density F . Luminosity is the measure of radiated energy per unit of time, measured in watts. Flux density describes the power of radiation through some surface, and it is given in units of Wm^{-2} . Spectral flux density can often be more useful, as it is the flux density for a certain wavelength. In SI units it is measured in $\text{Wm}^{-2} \text{nm}^{-1}$.

These quantities are sometimes given in non-SI units. Flux densities are usually very small, and are described in units of janskys ($1 \text{ Jy} = 10^{-26} \text{ W m}^{-2} \text{ Hz}^{-1}$). The CGS system is also commonly used. Energies are given in units of erg ($1 \text{ erg} = 10^{-7} \text{ J}$). And the spectral flux density in the CGS system can be measured in units of $\text{erg s}^{-1} \text{ cm}^{-2} \text{ \AA}^{-1}$.

The relation between flux density and luminosity is such that for an isotropically radiating star, the luminosity is the flux density spread along a spherical surface. So the formula for the relation is

$$L = 4\pi r^2 F, \tag{1}$$

where r is the distance from the star.

3.2 Magnitudes

Brightness of stars has been measured in magnitudes since antiquity, when Hipparchus classified stars visible with naked eye into six classes depending on their brightness. The brightest stars were magnitude 1, and faintest 6. This system has since been replaced by a more refined classification, where the ratio of bright-

nesses between two consecutive magnitudes is $100^{1/5}$ or about 2.512.

The magnitude system is relative, meaning that a measured magnitude is given as a relative difference between the magnitudes of the measured star and a comparison star. If we know the magnitude and flux of the comparison star, we can calculate the precise magnitude based on the flux density of our star using Pogson's formula

$$m_1 - m_2 = -2.5 \log \frac{F_1}{F_2}, \quad (2)$$

where m_1 and m_2 are the magnitudes, and F_1 and F_2 are the flux densities of the two stars. If two stars have magnitudes m and $m + 1$, and flux densities F_m and F_{m+1} , we can show that

$$m - (m - 1) = -2.5 \log \frac{F_m}{F_{m+1}} \Rightarrow \frac{F_m}{F_{m+1}} = 100^{1/5}. \quad (3)$$

Often a standard reference star is used for calibrating the magnitudes to a photometric system. Historically the star used has been Vega, for which the zero point magnitude was defined as 0 for all wavelengths. So if we know the flux density F_0 of the reference star, we can calculate the magnitude

$$m = -2.5 \log \frac{F}{F_0}. \quad (4)$$

Vega has been used as a reference star for the Johnson-Cousins UBVRI photometric system, which is described in more detail later.

The above magnitudes are *apparent magnitudes*. Because of the distance between the observer and the star, they do not represent the actual brightnesses of the stars. A very bright star will look dim if it is very far away. *Absolute magnitudes* have been defined as the apparent magnitude when the distance between the observer and the star is 10 parsecs. For example the apparent visual magnitude

of the Sun is -26.78 , but its absolute visual magnitude is 4.82 (Karttunen et al., 2016).

Photometry is usually performed in some restricted range of wavelengths defined by filters, which are discussed later in section 3.4.

3.3 Instrumental Magnitudes

The measured apparent magnitudes are dependent on the instruments used, and they should be calibrated to match some standard photometric system. The sensitivity of instruments varies for different wavelengths, and different instruments are used to measure different spectral bands (Karttunen et al., 2016). Survey data can be used to find the zero-point magnitude for the instrument, and then convert the instrumental magnitudes to the magnitude system of the survey. But first we need to actually get the instrumental magnitudes.

Unfortunately CCDs do not measure the flux directly, but instead the counts of photons that are detected by the instrument. But the counts can be used to approximate the fluxes, as the number of counts is proportional to the flux of a star.

There are two methods of measuring instrumental magnitudes: aperture photometry and point-source function fitting. Aperture photometry is fairly straightforward. A circular region (aperture) is fitted on a star in an image, so that all the light of the star is contained inside the aperture. The total flux can be thought as the sum of the counts from each individual pixel in the aperture. As images contain some background fluctuations, adjustments are needed. The background correction can be done by placing a ring-shaped region (annulus) so that it is around the aperture, but contains no neighbouring stars, as depicted in figure 2. The counts in the annulus are then normalized to the area of the aperture, and subtracted from the counts of the aperture to get the corrected value. The counts

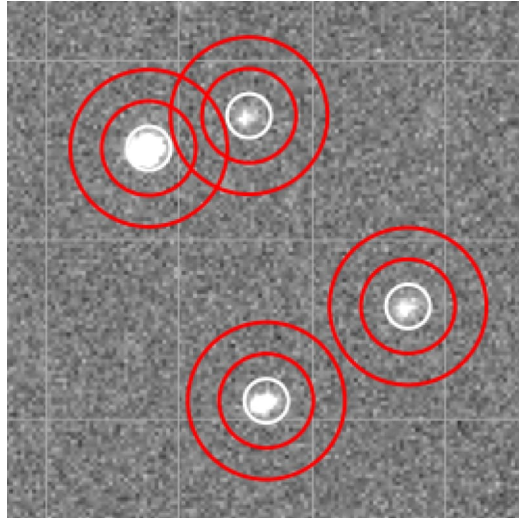


Figure 2: Apertures shown as white rings and annuli as red rings. Notice the upper annuli nearly intersecting with the apertures, and the slight overflow of light in the top-left aperture.

or flux can then be converted to magnitudes using the formulae described earlier (Palmer and Davenhall, 2001).

Point spread function (PSF) fitting is more complicated. It is useful for crowded regions where it is difficult to fit the apertures and annuli without catching nearby stars. Stars cannot actually be resolved by conventional telescopes. Instead, the images of stars are represented by the point spread functions of the telescope and atmospheric conditions, as illustrated in figure 3. Because of this, the shapes of all stars in the field are nearly identical. There can be some differences in the PSF caused by the edges of the field being off the optical axis, but for most telescopes this is not a problem. The light distribution of a CCD frame can be modelled using isolated stars. Using the distribution it is possible to model the stars by iteratively varying the positions and brightnesses of the model stars, until a replicate of the original image is produced. This method only works on detections that actually are the same shape. Extended objects, such as galaxies, will not work, as they are not point-sources (Palmer and Davenhall, 2001).

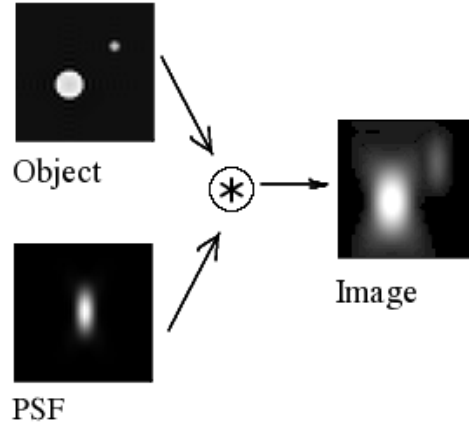


Figure 3: Effect of the point spread function on a point source and an extended object.

The acquired magnitudes then need to be calibrated to standard systems, so the results can be meaningfully compared with other data. Survey data can be used to find the instrument's zero-point magnitude by subtracting the magnitudes from the instrumental magnitudes of the survey. The calibrated magnitude is then acquired by adding the value zero-point. The full formula for calibrated magnitudes is

$$m_{calib} = m_{inst} - A + Z \quad (5)$$

where m_{calib} is the calibrated magnitude, m_{inst} is the instrumental magnitude, A is an arbitrary constant, Z is the zero point between standard and instrumental systems. (Palmer and Davenhall, 2001).

3.3.1 Atmospheric Extinction

As most astronomical observations are done on the ground, we need to take into account the effect of the atmosphere. The opacity of the atmosphere varies depending on the wavelength of electromagnetic radiation, as seen in figure 4. For visual wavelengths the opacity is low, but it quickly increases for shorter wave-

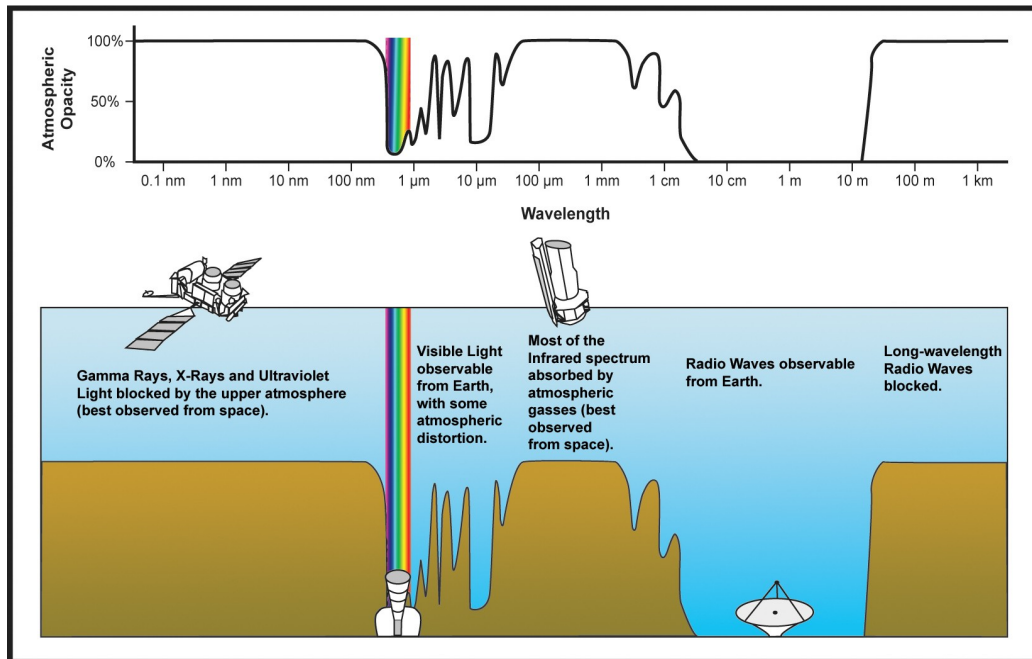


Figure 4: Opacity of the atmosphere for different wavelengths of the electromagnetic spectrum.

lengths in UV, X-ray, and gamma ray ranges. In IR ranges there are spikes of high opacity corresponding to absorption peaks of different components of the atmosphere. There is a window of low opacity in the radio wavelengths, but long-wavelength radio waves are blocked.

In addition to the wavelength of radiation, atmospheric extinction depends on airmass. It is a measure of how much air is between the observer and the observed target. The airmass is a function of the angle from zenith, air pressure, height of the atmosphere, etc (Karttunen et al., 2016, Palmer and Davenhall, 2001).

At zenith, the value of airmass is 1. It is defined as the quantity of air between the observer and the observed target. Near the zenith the airmass is defined simply as

$$X(z) = \sec(z), \quad (6)$$

where z is the angle from zenith. At large zenith angles, more complex effects

gain stronger effect. Refraction, curvature of the atmosphere, differences in air pressure and other variables need to be taken into account so detailed approximations can be made (Karttunen et al., 2016, Palmer and Davenhall, 2001). These approximations become more complicated than is necessary for this thesis. It is usually assumed that for zenith angles smaller than 70° the formula 6 is valid.

The measured magnitude is then the sum of the magnitude outside the atmosphere and the atmospheric extinction. A simple approximation for it is

$$m_0(\lambda) = m(\lambda) - k(\lambda)X(z), \quad (7)$$

Where $m(\lambda)$ is the magnitude depending on wavelength λ measured on the ground, $k(\lambda)$ is the coefficient of atmospheric extinction at wavelength λ , and X is the air-mass at zenith-angle z .

3.4 Photometric Systems and Surveys

There are two different types of photometric systems: absolute systems (AB) and systems based on some reference stars, often Vega. In Vega-based systems the colour of Vega between all wavelength bands is defined to be 0. In reality this is not true, as the spectral energy distribution of Vega is not flat (Budding, 2007). The AB system was developed later, and is based on flux measurements in absolute units.

The AB magnitude of a star is

$$AB = -2.5 \log(f) + 48.60, \quad (8)$$

where f is the flux density of the star in units of $\text{erg s}^{-1} \text{cm}^{-2} \text{Hz}^{-1}$ (Oke and Gunn, 1983). From this we can calculate that for every passband the flux at mag-

nitude 0 is about 3631 Jy. So for a hypothetical zero-point source the spectral energy distribution would truly be flat.

3.4.1 Colour Corrections

Most photometric systems contain more than one band. Such systems are multi-colour systems, and for all multi-colour systems a set of colour indices can be defined. The colour index is the difference between magnitudes of a given object in two different bands (Karttunen et al., 2016).

Colour indices can be used for making corrections to the instrumental magnitudes when calibrating them to a standard system. It is generally needed when very high precision photometry is being conducted, or the instrumental and standard systems do not match well.

The equation 5 with colour correction included becomes

$$U = U_{inst} - Z_U + C_U(U - B) + k_U X \quad (9)$$

Here U is the calibrated magnitude in the U filter band, U_{inst} is the instrumental magnitude, Z_U is the zero point between the standard and instrumental systems, C_U is the colour-correction term that depends on the colour index $U - B$, k_U is the extinction coefficient and X is the airmass (Palmer and Davenhall, 2001).

3.4.2 Johnson-Cousins System

The Johnson-Cousins system is one of the earliest and most commonly used photometric systems, and it is based on Vega (Bessell, 2005). The spectral bands of the Johnson system are titled U, B, V, R, I (Karttunen et al., 2016). The bands correspond to ultraviolet, blue, visual, red and infrared. The properties of the filter bands were affected at least in part by the qualities of the used photomultipliers,

which were used to detect the incoming light.

The original R and I bands were proposed by Cousins to be replaced with R_c and I_c bands. They are modifications of the R and I photometric bands, and because of this alteration the system is now called the Johnson-Cousins system. The original red passbands of the Johnson system had difficulties measuring red wavelengths accurately with the photomultipliers that were used (Bessell, 2005). The effective wavelengths and widths of the bands are shown in table 1.

3.4.3 SDSS

Sloan Digital Sky Survey (SDSS) is a comprehensive survey that explores the structure of the Milky Way, evolution of galaxies, and the structure of the universe. The survey has observed over a million galaxies, quasars, and stars outside the galactic plane of the Milky Way (Alam et al., 2015). The SDSS photometric system was created using 158 relatively bright standard stars (Smith et al., 2002), and it is based on the AB system (Karttunen et al., 2016). The primary purpose of SDSS is the study of large-scale structure of the universe (Bessell, 2005). The survey covers about 35% of the sky, imaged in 2.5 degrees wide stripes. The survey began in 2000, and it is still ongoing.

The survey telescope filters were used in a vacuum causing layers in their filter coatings to shrink, which shifted the bands towards blue. Fortunately the filters provided to the US Naval Observatory (USNO) were not placed in a vacuum, and did not suffer the defects. Because of this there are now two non-identical systems, of which the USNO filters are denoted with primes ($u'g'r'i'z'$) (Bessell, 2005).

Table 1: Wavelengths and widths of the bandpasses in the different photometric systems.

UBVRI	λ (Å)	$\Delta\lambda$ (Å)	SDSS	λ (Å)	$\Delta\lambda$ (Å)	PS1	λ (Å)	$\Delta\lambda$ (Å)
U	3663	650	u'	3596	570	g	4810	1370
B	4361	890	g'	4639	1280	r	6170	1390
V	5448	840	r'	6122	1150	i	7520	1290
R	6407	1580	i'	7439	1230	z	8660	1040
I	7980	1540	z'	8896	1070	y	9620	830
						w	6080	5400

3.4.4 Pan-STARRS1

From the surveys described in this thesis, Pan-STARRS1 (Panoramic Survey Telescope and Rapid Response System) saw the most use when developing the Autophotometer program. It was chosen as the standard survey in the project because it covers the whole northern sky. Like SDSS, it is based on the AB system (Tonry et al., 2012).

Some of the goals of Pan-STARRS1 are searching for minor planets, especially Potentially Hazardous Asteroids, and conducting precise photometry and astrometry on the stars in our galaxy and the Local Group (Chambers et al., 2016). The magnitude limit of the survey is about 22.

Filter bands used in Pan-STARRS1 are named g, r, i, z, y, and w (Tonry et al., 2012). They are sometimes denoted with a subscript p1 (for example g_{p1}). The filter bands span the spectrum from 4000 Å to over 10000 Å. Details of the bandpasses are shown in the table 1. The w band is much wider than the others, overlapping the bands g, r, and i, and the band is used in surveying objects in the Solar System. The rest of the bands are used in the 3π steradian survey that covers the sky north of declination -30° (Chambers et al., 2016).

Table 2: Wavelengths and widths of the 2MASS bandpasses.

Filter	λ (μm)	$\Delta\lambda$ (μm)
J	1.235	0.162
H	1.662	0.251
K _s	2.159	0.262

3.4.5 2MASS

2MASS (Two Micron All Sky Survey) is an infrared survey of the whole sky. Performing measurements in infrared bands is more difficult than in optical and UV ranges, because of the nonlinear absorption of infrared light in the atmosphere. The photometric system of 2MASS uses three filters: J, H, and K_s. They are chosen so that they overlap with the regions of low atmospheric opacity. The 2MASS survey telescope performed the imaging of each field in all filters simultaneously, using three different optical paths for each camera. 2MASS can detect objects with magnitudes up to 16 on the most sensitive filter (Skrutskie et al., 2006). The data release of the survey was published in 2003.

Objectives of the 2MASS survey were study of the Milky Way by detecting cool stars on the far side of the galactic disk, finding galaxies within the zone of avoidance (the region of the sky where the light of the Milky Way blocks observations in the visual bands). 2MASS is also capable of discovering brown dwarfs and observing the large-scale structure of the universe. Attributes of the 2MASS filter bandpasses are shown in table 2 (Cohen et al., 2003).

3.4.6 Transformations between systems

Sometimes it is necessary to transform instrumental magnitudes from a photometric system to another. For example if your telescope uses UBVRI filters but you want to compare the magnitudes to data from Pan-STARRS.

Various transformation formulae have been created by different researchers.

One set of transformations between SDSS and Johnson-Cousins systems has been described in an article by K. Jordi et al (2006). They provide transformation formulae both dependent and independent of metallicity. The deviations between calculated and measured magnitudes are about 0.01 or less, becoming larger with fainter magnitudes (Jordi, K. et al., 2006).

Transformation equations from Pan-STARRS filters to Johnson-Cousins system have been derived by Kostov and Bonev (2018). With Autophotometer we wanted to compare images using the Johnson-Cousins system to magnitudes from Pan-STARRS. Described below are the equations that were used in the program.

$$B = g + 0.199 + 0.540(g - r) + 0.016(g - r)^2 \quad (10)$$

$$V = r - 0.017 + 0.492(g - r) \quad (11)$$

$$R = r - 0.166 - 0.275(r - i) \quad (12)$$

$$I = i - 0.416 - 0.214(r - i) \quad (13)$$

The standard deviations between converted magnitudes and true magnitudes are

$$\sigma_B = 0.056$$

$$\sigma_V = 0.032$$

$$\sigma_R = 0.038$$

$$\sigma_I = 0.061.$$

These equations were devised using faint stars, with magnitudes less than 19 (Kostov and Bonev, 2018). Therefore they suited well for the project that is described in the next section, as stars of similar magnitudes were examined there.

4 Program

4.1 Description

Autophotometer is a semi-automatic Python based pipeline for photometric measurements. It uses Source Extractor and SCAMP³ to find the detections from the user's FITS images, and finds matches for them from an online database. Autophotometer's objective is to provide a quick and easy way to study variable and transient stars, but can be used for other types of objects as well.

4.1.1 Supported Observatories and Filters

Autophotometer is intended to be used with images from Nordic Optical Telescope (NOT), but might also work with images obtained by other telescopes. Supported instruments are ALFOSC (including FASU), NOTCam and StanCam. It uses databases Pan-STARRS1 and 2MASS for calibration. Supported filter bands include BVRI, JHK_s, and Pan-STARRS grizy. Support for new observatories, instruments, databases, and filters will likely be added in future versions.

4.2 Installation

4.2.1 Requirements

Autophotometer requires SExtractor version $\geq 2.25.0$ ⁴ and SCAMP version $\geq 2.10.0$ ⁵, and their software requirements. Additionally it uses the following python packages:

- Astropy

³<https://www.astromatic.net/software/>

⁴<https://github.com/astromatic/sExtractor>

⁵<https://github.com/astromatic/scamp>

- Numpy
- Matplotlib
- Scipy
- Configparser
- photutils
- CCDProc
- Plotille
- Requests

Autophotometer was developed using Python 3.8, but any version that supports the required packages can be used to run it.

4.2.2 Setup - Using pip

Installation can be done using pip. Simply download the files from github⁶ and install the program using command "pip install ." in the directory of the downloaded files. The use of flag --user is recommended, so the program is installed for only the current user. It should be noted that when installing in a virtual environment, --user is not necessary.

The program itself can be run using the command AUTOPHOTOMETER. This is considered the "correct" way of installation, and the examples in the following sections expect that the program has been installed using pip.

When run, Autophotometer looks for the configuration files in the directory where the program is run. If it does not find them, the program looks for directory ~/.autophotometer, where pip created the files on installation.

⁶<https://github.com/almattil/autophotometer>

4.2.3 Setup - Manual

The files can be manually extracted into a directory and the program can be executed from there. The program tries to look for the configuration files in the directory where the program is run from. If they are missing, it looks for the directory `~/autophotometer`. The configuration files must exist in one of these locations, or the program will not run.

4.3 Usage

Autophotometer currently has two modes: single image and dual image operations. In single mode the program processes only one image, and in dual mode it runs two images of the field in different filter bands. Dual image mode compares the images to each other and outputs values for the detections in both images.

The dual mode is more constricted, as it only uses detections present in both images, which can cause some issues. The dual image functionality may be removed in future, as the single image mode gives more reliable results.

Running the program is done using the terminal. It can be called from any directory using the command:

```
AUTOPHOTOMETER [images]
```

Parameter "images" can contain up to two FITS files, depending on which mode you want to use. The program finds the used filter bands from the fits headers, and will give an error if a filter is unsupported. The fits header must contain certain keywords for SCAMP to be able to process them.

Autophotometer then asks if the user wants to make modifications to the fits files. It can create a backup of the original file, remove cosmic rays, and do the coordinate correction. The query screen is shown in figure 5.

```
*****
autophot: ver. 20210906

Filter 1: J
Do you want to make changes to SDSS0748_J1.fits before continuing?
[y]es, [n]o, [q]uit.
y/n/q: y
Do you want to make a backup of the file?
y/n: n
Do you want to remove cosmic rays?
y/n: n
Do you want to do the coordinate correction?
y/n: y
```

Figure 5: Autophotometer’s startup view in terminal, asking the user if they want to modify the image.

After the modifications, the program outputs histograms created by Plotille, shown in figures 6 and 7. The first histogram shows all the FWHM values of the detections in arcseconds. In the second histogram only the detections within a threshold are kept. This is done to exclude detections with too big or small FWHM, which might be galaxies, clusters, cosmic rays, or other non-star objects. The detections that are left are most likely stars.

Then the program shows a figure of the colour term calculations, such as depicted in figure 8. In the figure the X-axis shows the difference in magnitudes between two adjacent filters and the Y-axis shows the uncorrected instrumental magnitudes. A linear fit to the data is used to find the extinction coefficient and zero point magnitude. The figure can be used to evaluate whether the fit is good or not.

Finally the program draws the fits image, with markers depicting the different detection types and if the detections are present in the database. An example image is shown in figure 9. Note that in the figure, some detections are left unmarked. The detection threshold can be adjusted in the `conf_autophotometer.ini` file.

When a marker is clicked, the program outputs the coordinates of the detected

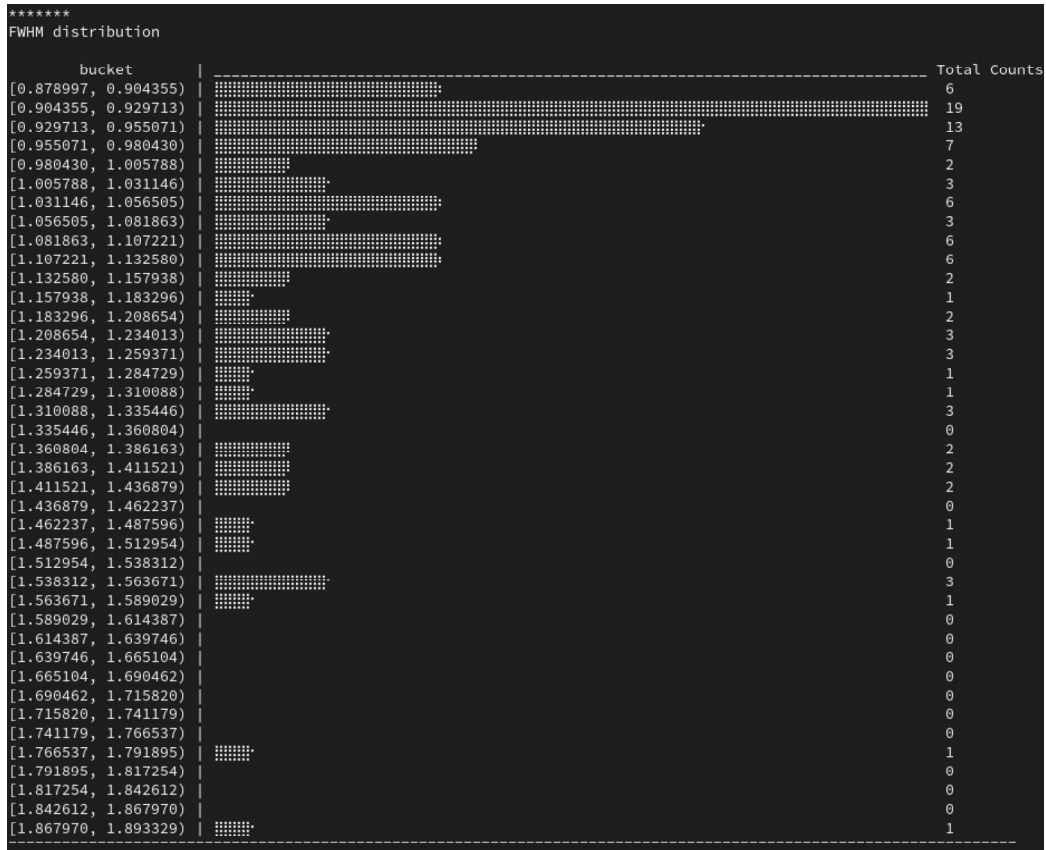


Figure 6: Example of a histogram produced by the program.

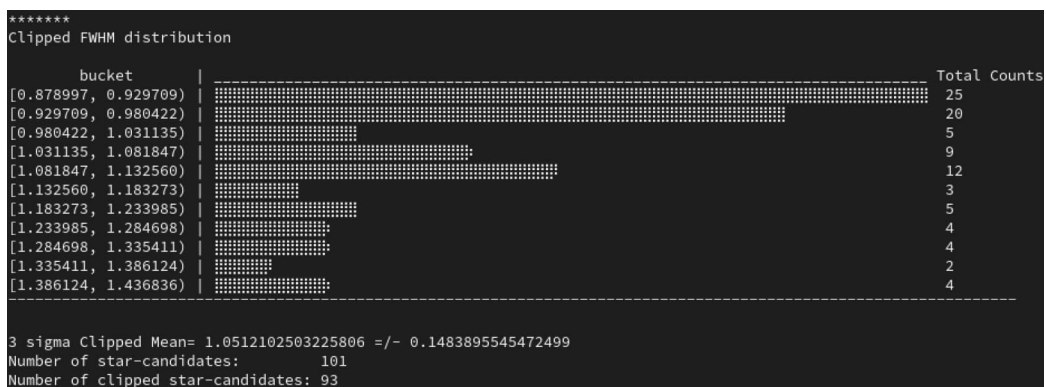


Figure 7: Clipped version of the histogram from figure 6. Notice that the bucket sizes have changed. Some statistics of the set is printed below the histogram.

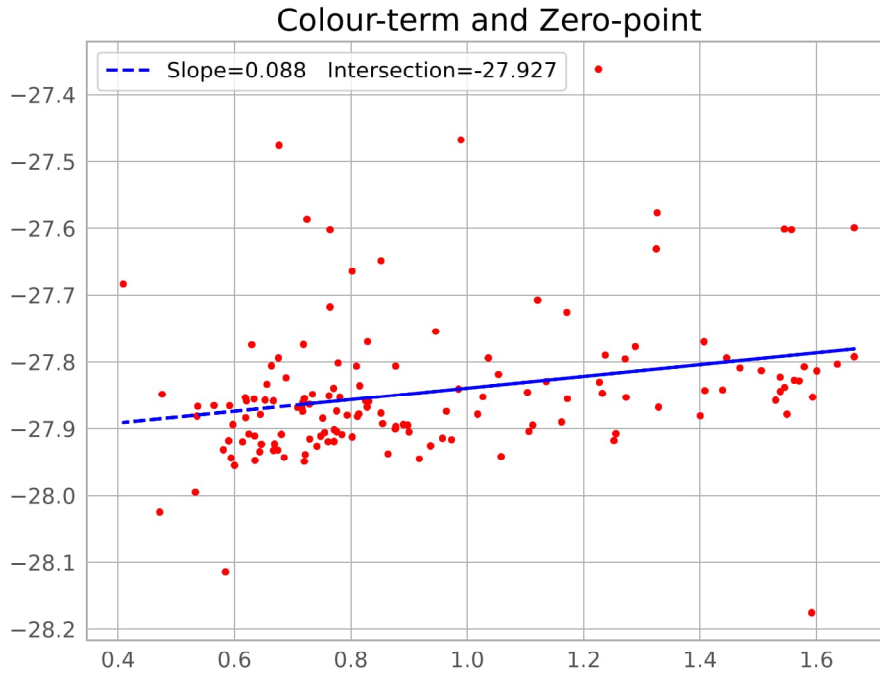


Figure 8: Colour term fit drawn by the program. The X-axis shows the colour difference and Y is the instrumental magnitude.

source in degrees, magnitudes, database magnitudes, and errors in the terminal. The program also saves the information of the selected detections and writes it into a file called "Selected_Mags_[image name].dat," which is generated in the directory where the program is executed.

4.4 API Documentation

In this section all the primary functions of the program are described. The basic workflow of the pipeline is described in figure 10.

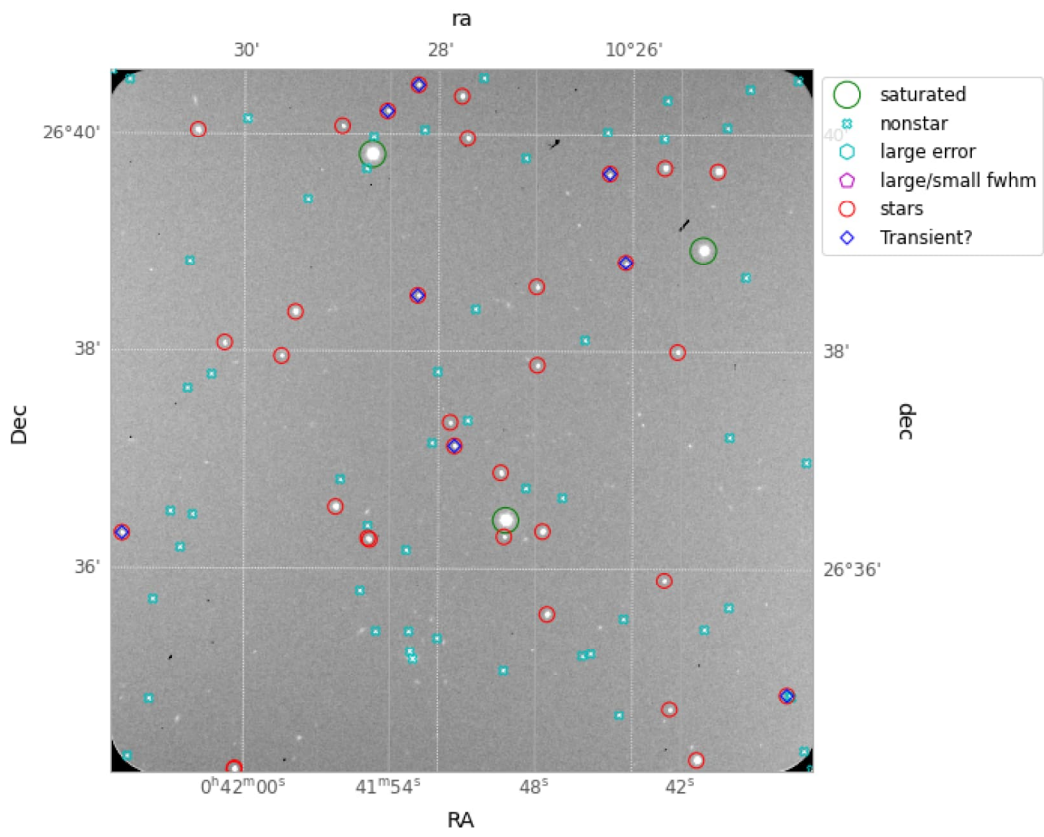


Figure 9: An example of a FITS image with overlays produced by Autophotometer.

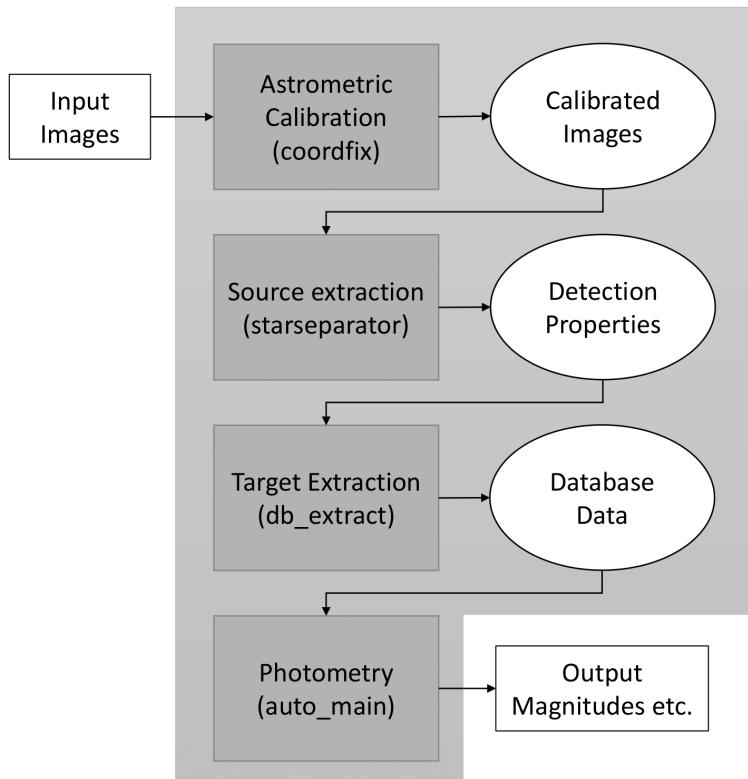


Figure 10: Autophotometer workflow diagram.

4.4.1 Coordinate correction

Coordinate correction is done using SCAMP. First the program runs Source Extractor, which generates a catalogue file for SCAMP. To function correctly, SCAMP requires that the FITS headers contain keywords providing WCS coordinates, image dimensions, and other qualities. The fits headers can in some cases be edited manually, or using external scripts, to fit the format that SCAMP requires.

SCAMP generates a file containing fits header keywords and their updated values. These values are then used to overwrite the originals, using Astropy's fits handling functions. The program reads the generated header keywords, and compares them to the original header. If a keyword is already present, it is deleted

before adding the updated keyword. This is done to prevent duplicate keywords which appeared when trying to update the header without deleting originals. This might have been caused by errors in the code or a bug in the function, but this way it works in every case.

This function creates modifications to the fits header, so creating a backup is recommended. Before the program does anything, it asks if the user wants to create a backup of the used file.

4.4.2 Cosmic ray removal

Cosmic rays are removed from images using the L.A. Cosmic technique provided by ccdproc Python package. It is a fast and simple function, which only needs the fits image data, readout noise, and the gain of the image. In some cases the images have multiple keywords for gain, and in those cases only the first is used. If gain is not found in the header, it was set to 1 for the purposes of this function. Cosmic ray removal is not needed with filters J, H, and K_s.

The function produces a new cleaned version of the fits image, which is then written over the original data. This creates irreversible modifications to the file, so making a backup is recommended.

4.4.3 Star separation

The program attempts to separate stars from other detections. It first takes the output catalog of the first run of Source Extractor, and uses it to find the mean FWHM. It only includes detections under the magnitude error limit, that are not saturated, and that have the CLASS_STAR parameter greater than the threshold. The thresholds for error of magnitude and the CLASS_STAR parameter can be edited from the conf_autophotometer.ini file in the ~/.autophotometer/ directory.

The CLASS_STAR parameter is an estimate of how likely a detected object

is a star. The closer it is to 1, the more likely it is a star. The closer a detection is to the magnitude limit, the less accurate the parameter will be. This limit depends on the image. In this document the parameter is often called star/galaxy or S/G parameter, as it is used for separating stars from galaxies and other extended objects.

It then runs Source Extractor again using the mean FWHM as the seeing. This increases the accuracy of the values from Source Extractor. This time the output catalogue also includes the coordinates in both pixels and right-ascension and declination, FWHM in pixels and arcseconds, S/G parameter, instrumental magnitudes and their errors, flux, and flags that describe for example if a detection is saturated.

Next a histogram of the FWHMs of the detections is drawn, and the list of FWHM values is sigma clipped. So only the values that are within three standard deviations are included.

Using these parameters the program separates from the catalogue all the detections that are flagged as saturated, whose S/G parameter is lower than the threshold, which by default is 0.8; that have errors of magnitude larger than twice the limit, which by default is 0.05; and whose FWHM deviates past the maximum or minimum of sigma-filtered FWHM values. What remains is added to a new array that contains only the detections that are most likely stars. The numbers of all other detections are also printed in the terminal.

4.4.4 Database access and coordinate matching.

The program finds the approximate center of the image using the median coordinates of all detections. For both databases the program performs a cone search, with the radius of the cone being 0.1 degrees by default. This should be enough for most images, but the value can be changed in the configuration file.

The query then receives the data from the database using Requests. The used database is automatically determined by the image's filter. If the filters are J, H, or K_s the queried database is 2MASS. In other cases Pan-STARRS1 is used.

The requested data contains magnitudes and their errors in the grizy filters from PS1, and JHK_s filters from 2MASS, depending which filters are used. Additionally the coordinates of the detections are extracted. The data is converted to an ascii table, and the columns are extracted into separate arrays for further processing.

If the image uses BVRI filters, the PS1 magnitudes are converted to the Johnson-Cousins system too. Details on the transformation formulae are described in section 3.4.6. In these cases the error of magnitude is the largest of either the magnitudes used in the transformation, or 0.05, which is approximately the error caused by the transformation.

The catalogue matching is done using `match_coordinates_sky` function from Astropy. The maximum separation of the coordinates is 1 arcsecond. After matching the catalogues, it determines if the detections are present in the database. If the detection is present, it gains flag 1. If not, it is flagged with 0. This makes it easier to later mark transients and other detections that cannot be found in the database.

The data is then gathered into a single array that contains the RA, DEC coordinates, the presence flag, measured magnitudes, database magnitudes, and database magnitude errors. The magnitudes in all the different filter bands are also gathered into their own array, for use in the photometry calculations.

4.4.5 Photometry calculations

When all the data is extracted from the database, the program starts processing the FITS data to measure the magnitudes of the detections. Source Extractor has

already determined magnitudes using PSF fitting. Here the program calculates a second set of magnitudes using aperture photometry. It is up to the user to choose which set seems more accurate.

The program picks all detections that are determined to be stars, and that have errors of magnitude smaller than the threshold from the configuration file (0.05 by default). If the number of such stars is less than 5, a warning is given that the number of low-error stars is too small, and the threshold is increased by 0.05. This is repeated until the number of stars is at least 5, or the error threshold becomes 1.

Then the program finds the difference between the Source Extractor magnitudes and the database magnitudes by subtracting the latter from the former. The zero point magnitude is then acquired from the mean of the differences. For magnitudes with colour term corrections, this is done differently.

In the next step we repeat the process with the aperture photometry functions provided by Photutils package. Aperture sizes are defined as 1.4 times the mean FWHM (in pixels) of detections classified as stars. The annulus inner radius is 3 FWHM, and the outer radius is 5 FWHM. The default radii can be changed in the configuration files. Then the zero point magnitude is found similarly as with Source Extractor magnitudes, by subtracting the database magnitudes from calculated magnitudes. In the end we have two sets of magnitudes. One set was computed by SExtractor using PSF fitting, the other using aperture photometry from Photutils.

As the database magnitudes are extracted in all available filter bands from Pan-STARRS or 2MASS, they can be used to find the colour correction terms. A linear fit to the data is made, an example of which was shown in figure 8. The horizontal axis is the colour index of a star, and vertical axis shows the difference between measured and database magnitudes. Colour indices for the used photometric systems are shown in table 3.

Table 3: Filters and corresponding colour indices in all available systems.

Pan-STARRS		Johnson-Cousins		2MASS	
Filter band	Colour	Filter band	Colour	Filter band	Colour
g_{ps}	g-r	B	B-V	J	J-H
r_{ps}	g-r	V	B-V	H	J-H
i_{ps}	r-i	R	V-R	K_s	J- K_s
z_{ps}	i-z	I	V-I		
y_{ps}	z-y				

The slope of the linear fit shows the dependency of colour on the magnitude, and the intersection of the linear fit and 0 is the zero-point magnitude. The colour correction term of a star is calculated as

$$CT = m \times CI + Z,$$

where m is the slope, CI colour index, and Z is the intersection with 0. This colour term is then subtracted from the magnitudes measured using Source Extractor and Photutils, and we get colour-corrected magnitudes.

4.4.6 Plotting

The image and database data is stored in a numpy array. The values of the array can be accessed by clicking detections in the image drawn by Autophotometer. Astropy functions are used to extract the relevant data, which are then used by matplotlib to produce the image. The data is scaled using zscale algorithm to better show the details of the image, and a coordinate overlay is created, again using astropy.

The different types of detections are then plotted on the image, overlaid on the fits data. Additionally, for each detection a small white marker is drawn. When such a marker is clicked, the program prints the information of the detection in the terminal. The data is fetched from the array by the index of the detections. Figure

9 shows what the images produced by the program look like, and the terminal output is shown in figure 11. The selected detections are also saved into a separate file after the image is closed.

Because calculating the colour term is not that simple and the results are not always reliable, the magnitudes without colour corrections are also given. It is up to the user to decide whether to use the magnitudes with or without the colour term.

Index	RA	DEC	DB_mag	DB_err	SEX_mag	SEX_noCT	SEX_err	Ph_mag	Ph_noCT	Star?
232	116.869738	6.852058	18.479	0.050	18.446	18.471	0.020	18.057	18.521	Likely
183	116.869938	6.868181	20.084	0.050	20.027	20.039	0.044	19.607	20.058	Likely
177	116.845596	6.875061	19.234	0.050	19.239	19.209	0.029	18.779	19.188	Likely
156	116.852731	6.874953	21.459	0.056	21.524	21.553	0.104	21.038	21.506	Nonstar
83	116.874063	6.825901	19.894	0.050	19.774	19.780	0.039	19.431	19.877	Likely
96	116.870488	6.832144	21.452	0.138	21.330	21.327	0.090	21.106	21.543	Nonstar
173	116.899257	6.876155	20.129	0.050	20.035	20.057	0.044	19.684	20.145	Likely
138	116.825419	6.890611	12.332	0.050	12.708	12.708	0.001	11.973	12.412	Bad FWHM
43	116.836934	6.807477	19.960	0.050	19.861	19.892	0.041	19.504	19.973	Likely
27	116.838232	6.798457	18.029	0.050	17.925	17.905	0.016	17.546	17.965	Likely
26	116.831158	6.797302	20.206	0.050	20.113	20.142	0.047	19.749	20.217	Likely

Figure 11: Information of some selected detections printed in the terminal.

5 Practical use of the pipeline

5.1 Short scientific background

The goal of this project was to develop an automatic pipeline for accurate photometry. The produced data could then be used to analyse spectral energy distributions (SEDs) of stars to identify different types of cataclysmic variable stars. Cataclysmic variables (CVs) are binary systems that occasionally show increases in brightness. They are interacting binary systems with a white dwarf primary and a low mass secondary donor star that has filled its Roche lobe, allowing mass transfer from the secondary to the white dwarf.

The stream of mass forms an accretion disc around the white dwarf. When the accretion disc is fully formed, the stream of mass contacts the edge of the disc,

heating the impact spot, which can become brighter than the stars and the disc. In some cases the white dwarf has a strong magnetic field that can disrupt or even prevent the formation of an accretion disc, and the stream impacts the star directly (Warner, 1995).

The theory of cataclysmic variables predicts that their period evolves from long to short orbital periods, and then bounce back to long orbital periods. The spectral energy distributions of such objects show logarithmically decreasing flux as the wavelengths become longer. Post-bounce objects show an increase in the flux density in IR wavelengths compared to the spectral energy distributions pre-bounce (Kato, 2015).

Spectral energy distributions of cataclysmic variables are composed of the SEDs of the white dwarf and the donor, and the accretion disc. As pre-bounce donors have increased flux densities in the infrared wavelengths, the otherwise flat SED of the white dwarf (in the IR spectrum) has an excess in the IR flux, creating a distinct feature in the SED. Theoretical SEDs of such objects are shown in figure 12 (Neustroev et al., 2018).

5.2 Process

A fairly large set of fits images of CVs from the Nordic Optical Telescope was ran through the pipeline. The images were taken with Johnson-Cousins BVRI, SDSS z', and 2MASS JHK_s filters.

Our targets needed to be identified from Autophotometer's images, in which all detections were highlighted. Aladin sky atlas software was used to find the detection and its coordinates by the target's name. In Autophotometer's image the coordinates of the cursor are shown in the bottom right corner of the window. So when the cursor was in Aladin's coordinates, it should point to the target.

The results are shown in tables 4 and 5. Table 4 contains the magnitudes

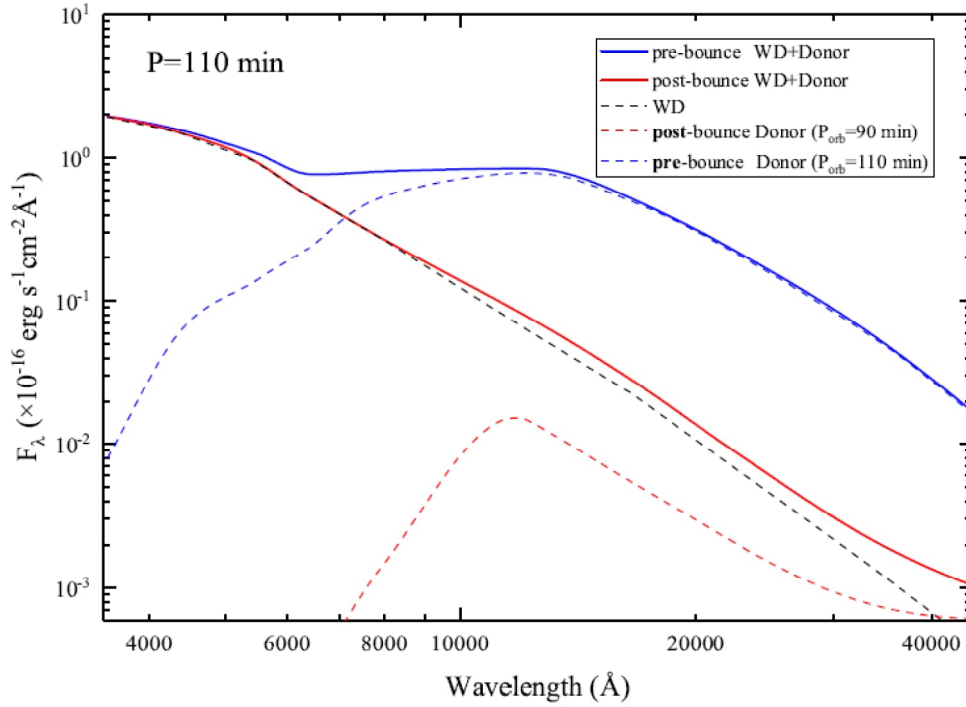


Figure 12: Theoretical spectral energy distributions. Figure from (Neustroev et al., 2018)

from Autophotometer. From the two magnitudes, calculated using PSF fitting and aperture photometry, the one closer to the database magnitude was selected for the table. The database magnitudes and their errors are shown in table 5.

Only few of the detections were imaged in all filters. In some cases getting reliable results was difficult because of various problems with either the images or the program. The issues are discussed in more detail in the following section.

Table 4: Calculated magnitudes and their errors

Name	B	Error	V	Error	R	Error	I	Error	Z	Error	J	error	H	error	Ks	error
ASASSN-13ae	19.93	0.05	19.79	0.04	19.70	0.05	19.49	0.03	-	-	19.45	0.03	18.92	0.04	-	-
ASASSN-14cl	18.78	0.02	18.55	0.02	17.97	0.02	18.35	0.02	18.35	0.02	17.13	0.01	16.69	0.01	16.29	0.02
ASASSN-14cv	19.49	0.05	19.39	0.04	19.35	0.04	19.31	0.04	19.99	0.05	19.44	0.06	18.87	0.07	-	-
ASASSN-14jq	20.60	0.06	20.27	0.04	20.04	0.04	19.89	0.03	-	-	19.38	0.05	18.53	0.03	18.22	0.07
ASASSN-14jv	19.23	0.03	19.19	0.03	19.07	0.02	18.92	0.02	19.49	0.03	18.79	0.03	18.12	0.03	17.79	0.07
ASASSN-16eg	-	-	-	-	-	-	-	-	-	-	17.69	0.02	17.26	0.02	16.85	0.04
ASASSN-15po	-	-	21.78	0.18	21.78	0.18	21.83	0.16	-	-	-	-	-	-	-	-
ASASSN-18ey	13.85	0.01	13.49	0.01	13.30	0.01	-	-	-	-	-	-	-	-	-	-
HO Cet	19.04	0.03	18.93	0.03	18.90	0.03	18.79	0.03	19.37	0.03	-	-	-	-	-	-
EI Psc	-	-	-	-	-	-	-	-	-	-	14.76	0.01	14.23	0.01	14.23	0.01
HT Cas	-	-	-	-	-	-	-	-	-	-	14.68	0.01	14.23	0.01	13.98	0.01
LL And	20.35	0.06	20.15	0.05	20.01	0.05	20.02	0.04	-	-	19.23	0.03	18.66	0.03	-	-
MisV1443	20.80	0.09	20.40	0.06	20.35	0.05	20.20	0.03	-	-	-	-	-	-	-	-
MOT 004527	19.46	0.04	19.24	0.03	18.98	0.03	18.48	0.02	18.65	0.02	17.18	0.01	16.59	0.01	16.29	0.02
OT J012059	19.92	0.04	19.78	0.04	19.87	0.04	20.00	0.04	-	-	20.38	0.08	-	-	-	-
OT J060009	-	-	20.17	0.04	-	-	19.84	0.04	-	-	-	-	-	-	-	-
OT 184228	20.80	0.07	20.47	0.05	20.25	0.05	20.44	0.04	-	-	-	-	20.14	0.11	-	-

Table 4: Calculated magnitudes and their errors

Name	B	Error	V	Error	R	Error	I	Error	Z	Error	J	error	H	error	Ks	error
OT J213806	16.23	0.01	16.12	0.01	15.91	0.01	15.74	0.01	16.15	0.01	15.00	0.01	14.46	0.01	14.09	0.01
OT 230523	19.98	0.08	19.70	0.07	19.63	0.07	19.38	0.06	-	-	18.85	0.04	19.04	0.05	-	-
QZ Lib	19.23	0.03	18.92	0.02	18.75	0.02	18.73	0.02	19.25	0.03	18.23	0.04	18.11	0.04	-	-
SDSS 145758	19.95	0.03	19.82	0.03	19.72	0.03	19.77	0.02	-	-	19.28	0.08	18.80	0.07	-	-
SDSS 161027	-	-	-	-	-	-	-	-	-	-	19.10	0.04	19.18	0.05	18.11	0.07
SDSS 220553	20.56	0.08	20.35	0.08	20.60	0.09	20.02	0.05	-	-	19.79	0.06	19.35	0.06	18.46	0.08
UZ Boo	20.28	0.04	20.17	0.03	19.87	0.03	19.84	0.03	-	-	19.72	0.07	18.52	0.06	-	-
V344 Lyr	18.93	0.02	18.80	0.02	18.56	0.02	18.16	0.02	18.44	0.02	17.73	0.01	17.00	0.01	17.00	0.03
V355 UMa	17.34	0.02	17.41	0.02	17.44	0.02	17.61	0.02	18.16	0.02	17.48	0.02	17.04	0.01	16.55	0.02
V466 And	20.61	0.07	20.38	0.05	20.21	0.04	19.89	0.03	-	-	19.73	0.05	19.50	0.07	18.89	0.10
V2176 Cyg	20.59	0.07	20.32	0.04	20.23	0.04	20.15	0.03	-	-	20.38	0.13	-	-	-	-
V1504 Cyg	-	-	-	-	-	-	-	-	-	-	14.69	0.01	14.62	0.01	14.43	0.01
WZ Sge	-	-	-	-	-	-	-	-	-	-	14.85	0.01	14.58	0.01	13.93	0.01
ASASSN-15bp	20.62	0.05	20.38	0.03	20.20	0.04	20.15	0.03	-	-	19.97	0.06	19.72	0.08	-	-
ASASSN-18ey	14.52	0.01	14.25	0.01	13.85	0.01	13.53	0.01	-	-	-	-	-	-	-	-
ASASSN-19de	16.74	0.01	16.42	0.01	16.08	0.01	15.53	0.01	-	-	15.23	0.01	15.01	0.02	14.64	0.02

Table 4: Calculated magnitudes and their errors

Name	B	Error	V	Error	R	Error	I	Error	Z	Error	J	error	H	error	Ks	error
ASAS J102522	19.43	0.04	19.29	0.03	18.96	0.03	18.86	0.03	-	-	17.78	0.02	17.43	0.01	16.83	0.03
CRTS J104411	19.63	0.03	19.52	0.03	19.39	0.03	19.24	0.03	-	-	18.59	0.03	18.61	0.03	18.33	0.05
EG Cnc	19.03	0.02	18.73	0.03	18.75	0.02	18.64	0.02	19.07	0.03	18.17	0.02	17.32	0.02	16.52	0.05
GW Lib	16.84	0.02	16.82	0.02	16.73	0.01	16.62	0.01	17.19	0.01	16.24	0.04	15.82	0.04	15.59	0.06
HV Vir	19.37	0.03	19.18	0.02	19.06	0.02	18.91	0.02	19.34	0.03	18.38	0.03	17.88	0.03	17.62	0.05
IK Leo	20.51	0.05	20.50	0.04	20.50	0.04	20.36	0.03	-	-	19.79	0.06	19.12	0.08	18.66	0.09
MT Com	-	-	-	-	-	-	-	-	-	-	19.25	0.05	18.67	0.04	18.23	0.05
OT J062703	20.67	0.05	20.25	0.04	20.19	0.04	20.10	0.03	-	-	19.33	0.05	18.74	0.05	16.54	0.02
QZ Lib	-	-	-	-	-	-	-	-	-	-	18.39	0.03	18.42	0.10	17.50	0.04
PNV J172929	21.92	0.12	22.01	0.10	20.87	0.08	20.71	0.08	-	-	-	-	-	-	-	-
RZ Leo	18.53	0.01	18.27	0.01	18.10	0.01	17.56	0.01	17.82	0.01	16.26	0.01	16.07	0.01	15.55	0.01
SDSS1238	18.00	0.02	17.81	0.02	17.78	0.02	17.69	0.01	18.07	0.01	17.40	0.02	16.78	0.02	15.86	0.05

Table 5: Database magnitudes and their errors

Name	DB B	Error	DB V	Error	DB R	Error	DB I	Error	DB Z	Error	DB J	error	DB H	error	DB Ks	error
ASASSN-13ae	19.95	0.06	19.79	0.06	19.70	0.05	19.59	0.05	-	-	-	-	-	-	-	-
ASASSN-14cl	19.09	0.05	18.72	0.05	18.38	0.05	17.73	0.05	18.48	0.03	-	-	-	-	-	-
ASASSN-14cv	19.40	0.05	19.28	0.05	19.19	0.07	18.99	0.07	19.55	0.04	-	-	-	-	-	-
ASASSN-14jq	20.62	0.05	20.31	0.05	20.14	0.05	19.94	0.05	-	-	-	-	-	-	-	-
ASASSN-14jv	19.25	0.05	19.17	0.05	19.15	0.05	19.08	0.05	19.50	0.02	-	-	-	-	-	-
ASASSN-16eg	-	-	-	-	-	-	-	-	-	-	-	-	-	-	-	-
ASASSN-15po	-	-	21.70	0.07	21.49	0.07	21.15	0.07	-	-	-	-	-	-	-	-
ASASSN-18ey	20.67	0.07	18.39	0.07	17.46	0.13	-	-	-	-	-	-	-	-	-	-
HO Cet	19.05	0.05	18.94	0.05	18.88	0.05	18.73	0.05	19.22	0.02	-	-	-	-	-	-
EI Psc	-	-	-	-	-	-	-	-	-	-	-	-	-	-	-	-
HT Cas	-	-	-	-	-	-	-	-	-	-	14.70	0.03	14.23	0.04	13.84	0.06
LL And	20.29	0.05	20.08	0.05	19.96	0.05	19.82	0.05	-	-	-	-	-	-	-	-
MisV1443	20.60	0.05	20.50	0.05	20.38	0.05	20.08	0.05	-	-	-	-	-	-	-	-
MOT 004527	19.19	0.05	18.72	0.05	18.47	0.06	18.31	0.06	18.10	0.03	-	-	-	-	-	-
OT J012059	19.37	0.14	19.58	0.14	19.67	0.06	19.52	0.06	-	-	-	-	-	-	-	-
OT J060009	-	-	20.20	0.05	-	-	20.04	0.05	-	-	-	-	-	-	-	-
OT 184228	20.70	0.05	20.27	0.05	20.12	0.05	20.18	0.05	-	-	-	-	-	-	-	-

Table 5: Database magnitudes and their errors

Name	DB B	Error	DB V	Error	DB R	Error	DB I	Error	DB Z	Error	DB J	error	DB H	error	DB Ks	error
OT J213806	16.43	0.05	16.02	0.05	15.85	0.05	15.83	0.05	13.89	0.04	-	-	-	-	-	-
OT 230523	19.97	0.05	19.70	0.05	19.17	0.05	17.69	0.05	-	-	-	-	-	-	-	-
QZ Lib	19.23	0.05	18.91	0.05	18.79	0.05	18.79	0.05	19.16	0.02	-	-	-	-	-	-
SDSS 145758	19.94	0.05	19.79	0.05	19.72	0.05	19.63	0.05	-	-	14.96	0.04	14.64	0.07	-	-
SDSS 161027	-	-	-	-	-	-	-	-	-	-	-	-	-	-	-	-
SDSS 220553	20.44	0.05	19.84	0.05	19.67	0.05	19.98	0.05	-	-	-	-	-	-	-	-
UZ Boo	20.26	0.05	20.00	0.05	19.88	0.05	19.83	0.05	-	-	-	-	-	-	-	-
V344 Lyr	18.96	0.12	18.85	0.12	18.67	0.11	18.14	0.11	18.18	0.40	15.61	0.05	15.43	0.10	15.28	0.15
V355 UMa	17.27	0.06	17.22	0.06	17.23	0.05	17.26	0.05	17.60	0.06	-	-	-	-	-	-
V466 And	20.44	0.06	20.04	0.06	19.88	0.06	19.89	0.06	-	-	-	-	-	-	-	-
V2176 Cyg	20.52	0.05	20.32	0.05	20.23	0.05	20.18	0.05	-	-	-	-	-	-	-	-
V1504 Cyg	-	-	-	-	-	-	-	-	-	-	16.11	0.09	15.91	0.15	15.40	-
WZ Sge	-	-	-	-	-	-	-	-	-	-	-	-	-	-	-	-
ASASSN-15bp	20.65	0.09	20.44	0.09	20.34	0.06	20.27	0.06	-	-	-	-	-	-	-	-
ASASSN-18ey	20.67	0.07	18.39	0.07	17.46	0.13	17.75	0.13	-	-	-	-	-	-	-	-
ASASSN-19de	19.75	0.05	19.37	0.05	19.07	0.05	18.53	0.05	-	-	-	-	-	-	-	-

Table 5: Database magnitudes and their errors

Name	DB B	Error	DB V	Error	DB R	Error	DB I	Error	DB Z	Error	DB J	error	DB H	error	DB Ks	error
ASAS J102522	19.45	0.05	19.27	0.05	19.15	0.05	18.92	0.05	-	-	-	-	-	-	-	-
CRTS J104411	19.62	0.05	19.39	0.05	19.28	0.05	19.22	0.05	-	-	-	-	-	-	-	-
EG Cnc	18.93	0.05	18.93	0.05	18.71	0.05	18.65	0.05	19.10	0.01	-	-	-	-	-	-
GW Lib	16.74	0.05	16.57	0.05	16.51	0.05	16.48	0.05	16.76	0.01	-	-	-	-	-	-
HV Vir	19.37	0.05	19.18	0.05	19.06	0.05	18.91	0.05	19.20	0.03	-	-	-	-	-	-
IK Leo	20.49	0.05	20.31	0.05	20.22	0.05	20.11	0.05	-	-	-	-	-	-	-	-
MT Com	-	-	-	-	-	-	-	-	-	-	-	-	-	-	-	-
OT J062703	20.97	0.06	20.23	0.06	19.99	0.06	20.26	0.06	-	-	-	-	-	-	-	-
QZ Lib	-	-	-	-	-	-	-	-	-	-	-	-	-	-	-	-
PNV J172929	21.73	0.07	21.20	0.07	20.90	0.07	20.64	0.07	-	-	-	-	-	-	-	-
RZ Leo	18.99	0.06	18.63	0.06	18.33	0.06	17.78	0.06	17.82	0.03	-	-	-	-	-	-
SDSS1238	18.05	0.05	17.80	0.05	17.69	0.05	17.62	0.05	18.06	0.01	-	-	-	-	-	-

5.3 Problems

5.3.1 Issues with data

SCAMP had problems processing some of the images. In some cases the images were incorrectly calibrated. The astrometric calibration of the detections especially near the edges of the field occasionally failed, as seen in figure 13. Usually the object of interest is near the center, and there are enough reference stars to calculate good magnitudes. Some images could not be processed at all, or the calibrated coordinates were completely incorrect. We could not determine the reason behind these issues.

The astrometric calibration of detections near the edges of the field occasionally failed, as seen in figure 13, where many stars are marked as transients. Usually the object of interest is near the center and there are enough reference stars to calculate good magnitudes, so this is not that big of a problem.

5.3.2 Dense fields

Sometimes the fields are very dense, as depicted in figure 13, or they can contain many false detections. In these cases the Photutils magnitude calculations can be inaccurate, as they are done using aperture photometry and there might not be enough empty space around the stars. Source Extractor accuracy was generally better in high-density fields. If there are many potentially spurious detections, increasing the detection thresholds can give better results.

5.3.3 Sparse fields

A low-density field is shown in figure 14. It can be seen that most of the detections are marked as "nonstar." This is most likely caused by Source Extractor's star/galaxy classifier, which is used to determine if a detection is a star or a galaxy

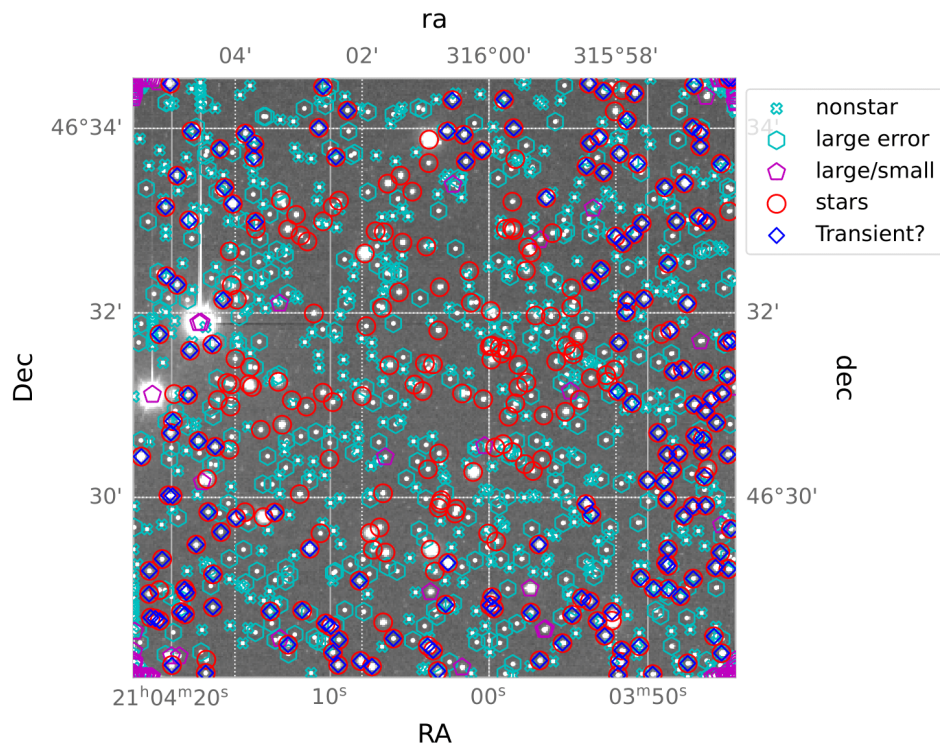


Figure 13: Image of a fairly dense field. In some images the astrometric calibration starts to fail for some objects near the edges of the field, causing them to be marked as transients.

(or other non-point source). The threshold for determining that a detection is a star can be changed in the configuration file. By adjusting it the user can likely cause more stars to be included in the photometry calculations, but the program might also select nonstar detections, causing errors. If the field has few galaxies or clusters, lowering the threshold is usually fine.

5.3.4 Locating targets

In some cases, especially with filter bands JHK_s , the target was not present in the database. This is not really a problem, as long as there are other stars that are present both in the image and the database. If the number of stars is too low, the calculated magnitudes can be inaccurate.

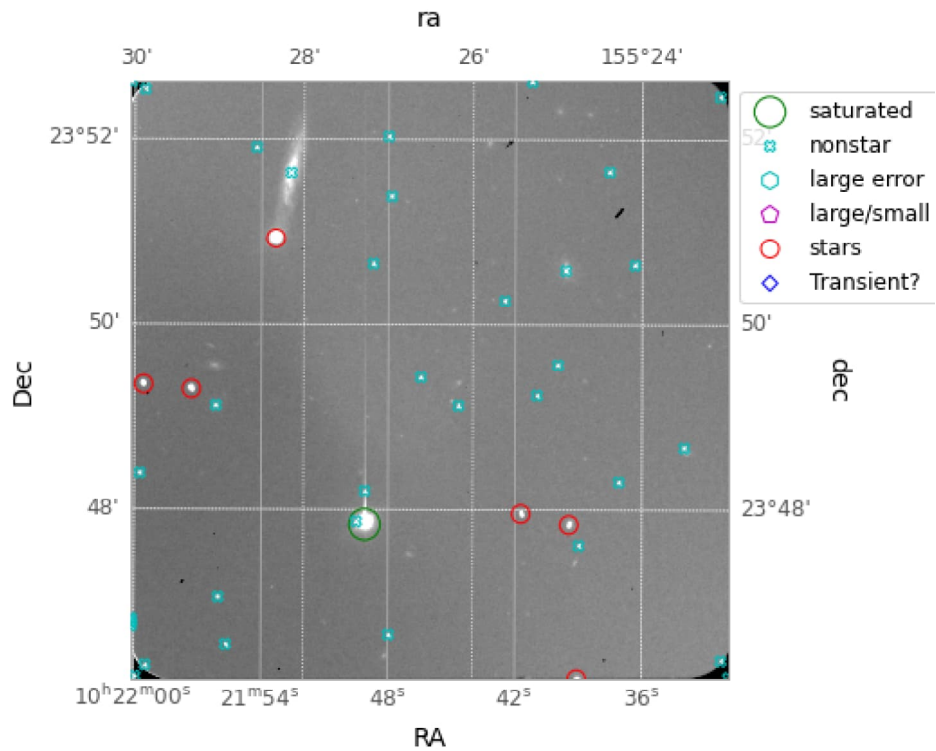


Figure 14: Image of a fairly sparse field. Only 6 detections are marked as stars, of which one is on the very edge of the field.

In the worst cases the target might not be visible at all because of bad observation conditions or image quality. Changing Source Extractor's threshold for detection in the configuration file of the program can help in some cases. Lowering the detection thresholds can cause low-accuracy detections to be detected. When doing so, increasing the strictness of the sigma clipping can reduce the errors that might be caused by inaccurate and nonstar detections. This method of course requires that the target is at least faintly visible on the image. In some images this was not the case.

5.3.5 Effects of the colour term

For dense fields the colour term becomes nearly zero, while for fields with low number of stars the value can be unrealistically large or small. The correct values for the colour term can be found on the NOT's websites⁷. Generally the value should be between -0.1 and 0.1, depending on the filter. The user can compare the program's results with those stated on the official site to determine whether or not to use the magnitudes with CT correction.

Lowering the sigma clipping multiplier can help with the accuracy of dense field magnitudes that include the colour term. Selection of specific stars as reference stars for the photometric calculations was discussed, but this feature is currently not implemented in the program.

The photometry calculations are performed differently when the colour term is included. In equation 5, the combined terms $m_{inst} - A + Z$ are acquired by extrapolating to 0 from a linear fit to the data. The data is often very scattered, so the fit can be inaccurate. Some adjustments could probably be made to the colour term calculations to get better results, but for now, it is up to the user to choose which magnitudes to use.

5.4 Results and Discussion

The deviations between image and database magnitudes across all detections in most fields were generally quite small (< 0.1 magnitudes). Source extractor's PSF fitting generally gives the most accurate data, but the aperture photometry magnitudes are not too inaccurate either. The inclusion of colour term is more complicated. In almost all infrared magnitudes the colour term was very far from 0, and in very few images overall the colour term was close to the values given in

⁷<http://www.not.iac.es/instruments/alfosc/zpmon/>

the NOT instrument's documentation on the internet.

Preliminary analysis of the SEDs shows that identifying period bouncers is possible using the data produced by Autophotometer. As seen in figure 15, the infrared excess is clearly visible in MOT 044527's spectral energy distribution, while V344 Lyr's SED is nearly linear in the logarithmic scale.

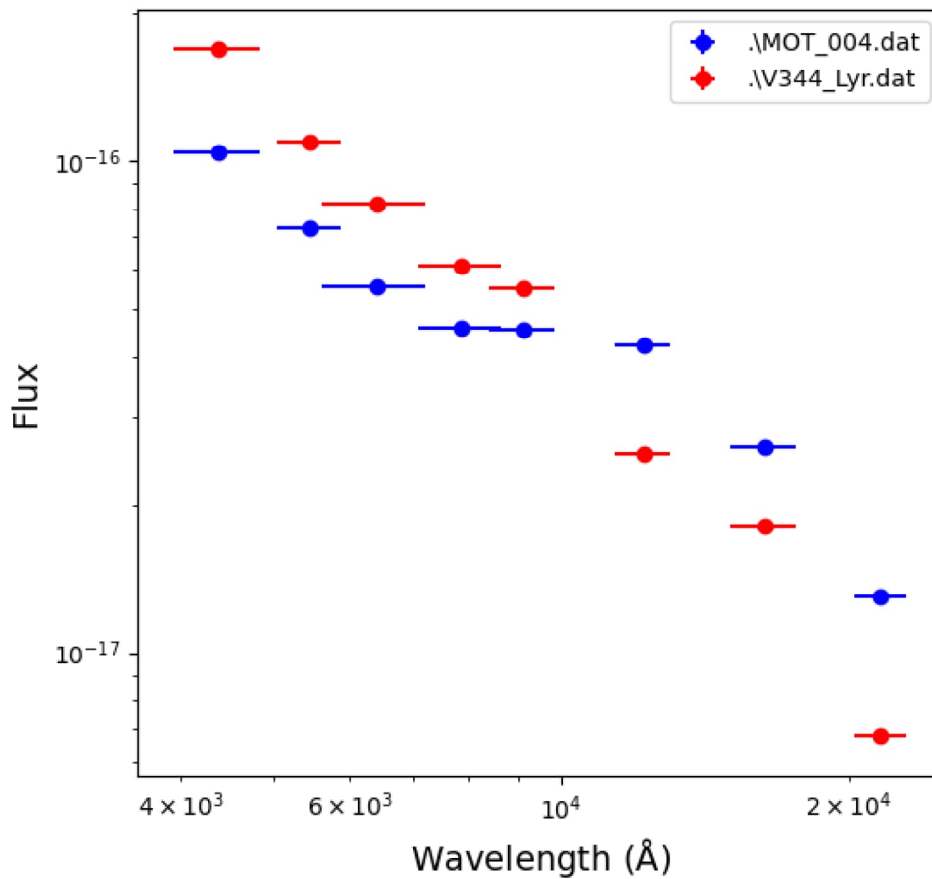
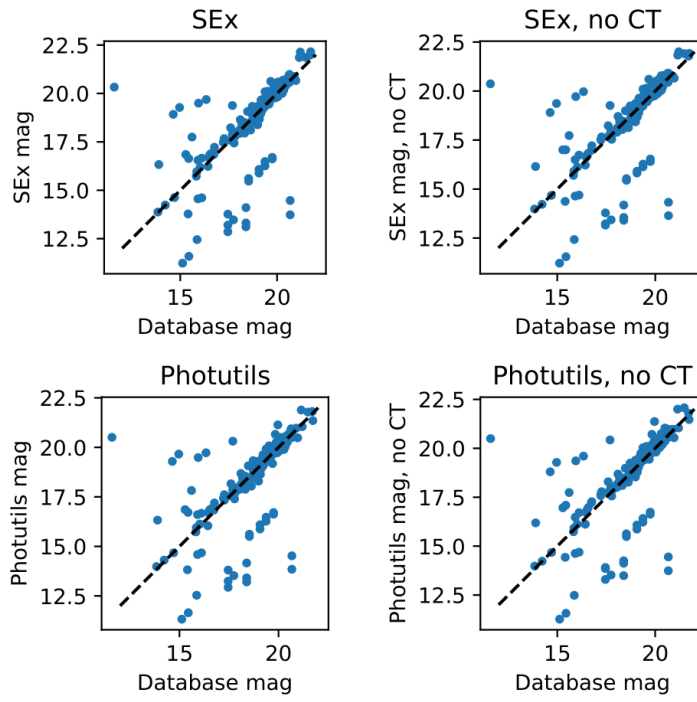


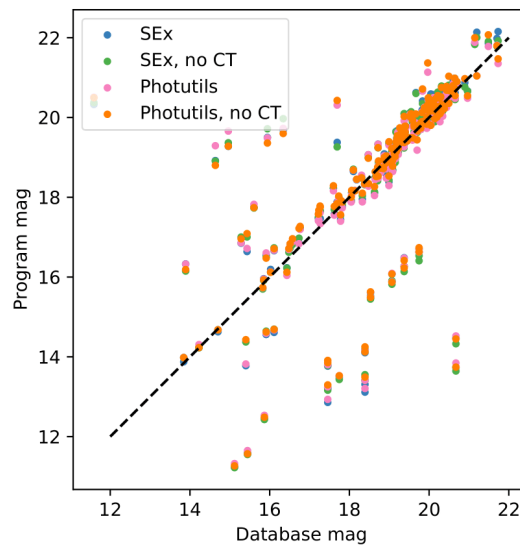
Figure 15: Spectral energy distributions of detections MOT 004527 and V344 Lyr.

Deviations from the database magnitudes are depicted in figures 16a and 16b. In the figures are displayed the calculated magnitudes against the database magnitudes of all detections in a single image. It is expected that magnitudes deviate

from the database magnitudes a little, as all stars are slightly variable. We can see that some of the measured magnitudes have quite large deviations. Most of the detections however match quite well with the databases. From figure 16b it can be seen that the differences between the different methods of photometric calculations are quite small.



(a)



(b)

Figure 16: (a) Comparison between measured and database magnitudes. (b) Figures from (a) combined into one figure, so the differences can be seen more clearly.

References

Alam, S., Albareti, F. D., Allende Prieto, C., Anders, F., Anderson, S. F., Ander-
ton, T., Andrews, B. H., Armengaud, E., Aubourg, É., Bailey, S., Basu, S.,
Bautista, J. E., Beaton, R. L., Beers, T. C., Bender, C. F., Berlind, A. A., Beut-
ler, F., Bhardwaj, V., Bird, J. C., Bizyaev, D., Blake, C. H., Blanton, M. R.,
Blomqvist, M., Bochanski, J. J., Bolton, A. S., Bovy, J., Shelden Bradley, A.,
Brandt, W. N., Brauer, D. E., Brinkmann, J., Brown, P. J., Brownstein, J. R.,
Burden, A., Burtin, E., Busca, N. G., Cai, Z., Capozzi, D., Carnero Rosell,
A., Carr, M. A., Carrera, R., Chambers, K. C., Chaplin, W. J., Chen, Y.-C.,
Chiappini, C., Chojnowski, S. D., Chuang, C.-H., Clerc, N., Comparat, J.,
Covey, K., Croft, R. A. C., Cuesta, A. J., Cunha, K., da Costa, L. N., Da Rio,
N., Davenport, J. R. A., Dawson, K. S., De Lee, N., Delubac, T., Deshpande,
R., Dhital, S., Dutra-Ferreira, L., Dwelly, T., Ealet, A., Ebelke, G. L., Ed-
mondson, E. M., Eisenstein, D. J., Ellsworth, T., Elsworth, Y., Epstein, C. R.,
Eracleous, M., Escoffier, S., Esposito, M., Evans, M. L., Fan, X., Fernández-
Alvar, E., Feuillet, D., Filiz Ak, N., Finley, H., Finoguenov, A., Flaherty,
K., Fleming, S. W., Font-Ribera, A., Foster, J., Frinchaboy, P. M., Galbraith-
Frew, J. G., García, R. A., García-Hernández, D. A., García Pérez, A. E.,
Gaulme, P., Ge, J., Génova-Santos, R., Georgakakis, A., Ghezzi, L., Gille-
spie, B. A., Girardi, L., Goddard, D., Gontcho, S. G. A., González Hernán-
dez, J. I., Grebel, E. K., Green, P. J., Grieb, J. N., Grieves, N., Gunn, J. E.,
Guo, H., Harding, P., Hasselquist, S., Hawley, S. L., Hayden, M., Hearty,
F. R., Hekker, S., Ho, S., Hogg, D. W., Holley-Bockelmann, K., Holtzman,
J. A., Honscheid, K., Huber, D., Huehnerhoff, J., Ivans, I. I., Jiang, L., John-
son, J. A., Kinemuchi, K., Kirkby, D., Kitaura, F., Klaene, M. A., Knapp,
G. R., Kneib, J.-P., Koenig, X. P., Lam, C. R., Lan, T.-W., Lang, D., Laurent,
P., Le Goff, J.-M., Leauthaud, A., Lee, K.-G., Lee, Y. S., Licquia, T. C., Liu,

J., Long, D. C., López-Corredoira, M., Lorenzo-Oliveira, D., Lucatello, S., Lundgren, B., Lupton, R. H., Mack, Claude E., I., Mahadevan, S., Maia, M. A. G., Majewski, S. R., Malanushenko, E., Malanushenko, V., Manchado, A., Manera, M., Mao, Q., Maraston, C., Marchwinski, R. C., Margala, D., Martell, S. L., Martig, M., Masters, K. L., Mathur, S., McBride, C. K., McGehee, P. M., McGreer, I. D., McMahan, R. G., Ménard, B., Menzel, M.-L., Merloni, A., Mészáros, S., Miller, A. A., Miralda-Escudé, J., Miyatake, H., Montero-Dorta, A. D., More, S., Morganson, E., Morice-Atkinson, X., Morrison, H. L., Mosser, B., Muna, D., Myers, A. D., Nandra, K., Newman, J. A., Neyrinck, M., Nguyen, D. C., Nichol, R. C., Nidever, D. L., Noterdaeme, P., Nuza, S. E., O’Connell, J. E., O’Connell, R. W., O’Connell, R., Ogando, R. L. C., Olmstead, M. D., Oravetz, A. E., Oravetz, D. J., Osumi, K., Owen, R., Padgett, D. L., Padmanabhan, N., Paegert, M., Palanque-Delabrouille, N., Pan, K., Parejko, J. K., Pâris, I., Park, C., Pattarakijwanich, P., Pellejero-Ibanez, M., Pepper, J., Percival, W. J., Pérez-Fournon, I., Pérez-Ràfols, I., Petitjean, P., Pieri, M. M., Pinsonneault, M. H., Porto de Mello, G. F., Prada, F., Prakash, A., Price-Whelan, A. M., Protopapas, P., Rad-dick, M. J., Rahman, M., Reid, B. A., Rich, J., Rix, H.-W., Robin, A. C., Rockosi, C. M., Rodrigues, T. S., Rodríguez-Torres, S., Roe, N. A., Ross, A. J., Ross, N. P., Rossi, G., Ruan, J. J., Rubiño-Martín, J. A., Rykoff, E. S., Salazar-Albornoz, S., Salvato, M., Samushia, L., Sánchez, A. G., Santiago, B., Sayres, C., Schiavon, R. P., Schlegel, D. J., Schmidt, S. J., Schneider, D. P., Schultheis, M., Schwobe, A. D., Scóccola, C. G., Scott, C., Sellgren, K., Seo, H.-J., Serenelli, A., Shane, N., Shen, Y., Shetrone, M., Shu, Y., Silva Aguirre, V., Sivarani, T., Skrutskie, M. F., Slosar, A., Smith, V. V., Sobreira, F., Souto, D., Stassun, K. G., Steinmetz, M., Stello, D., Strauss, M. A., Streblyanska, A., Suzuki, N., Swanson, M. E. C., Tan, J. C., Tayar, J., Terrien,

- R. C., Thakar, A. R., Thomas, D., Thomas, N., Thompson, B. A., Tinker, J. L., Tojeiro, R., Troup, N. W., Vargas-Magaña, M., Vazquez, J. A., Verde, L., Viel, M., Vogt, N. P., Wake, D. A., Wang, J., Weaver, B. A., Weinberg, D. H., Weiner, B. J., White, M., Wilson, J. C., Wisniewski, J. P., Wood-Vasey, W. M., Ye'che, C., York, D. G., Zakamska, N. L., Zamora, O., Zasowski, G., Zehavi, I., Zhao, G.-B., Zheng, Z., Zhou, X., Zhou, Z., Zou, H., and Zhu, G. (2015). The Eleventh and Twelfth Data Releases of the Sloan Digital Sky Survey: Final Data from SDSS-III. *Astrophysical Journal, Supplement*, 219(1):12.
- Bertin, E. (2006). Automatic Astrometric and Photometric Calibration with SCAMP. In Gabriel, C., Arviset, C., Ponz, D., and Enrique, S., editors, *Astronomical Data Analysis Software and Systems XV*, volume 351 of *Astronomical Society of the Pacific Conference Series*, page 112.
- Bertin, E. and Arnouts, S. (1996). SExtractor: Software for source extraction. *Astronomy and Astrophysics, Supplement*, 117(2):393–404.
- Bessell, M. (2005). Standard photometric systems. *Annual Review of Astronomy and Astrophysics*, 43:293–336.
- Bradley, L., Sipőcz, B., Robitaille, T., Tollerud, E., Vinícius, Z., Deil, C., Barbary, K., Wilson, T. J., Busko, I., Donath, A., Günther, H. M., Cara, M., krachyon, Conseil, S., Bostroem, A., Droettboom, M., Bray, E. M., Lim, P. L., Bratholm, L. A., Barentsen, G., Craig, M., Rathi, S., Pascual, S., Perren, G., Georgiev, I. Y., de Val-Borro, M., Kerzendorf, W., Bach, Y. P., Quint, B., and Souchereau, H. (2021). astropy/photutils: 1.2.0.
- Budding, E., -a., editor (2007). *An introduction to astronomical photometry*. Cambridge observing handbooks for research astronomers. Cambridge Uni-

versity Press, Cambridge, second edition edition. Title from publisher's bibliographic system (viewed on 05 Oct 2015).

Chambers, K. C., Magnier, E. A., Metcalfe, N., Flewelling, H. A., Huber, M. E., Waters, C. Z., Denneau, L., Draper, P. W., Farrow, D., Finkbeiner, D. P., Holmberg, C., Koppenhoefer, J., Price, P. A., Rest, A., Saglia, R. P., Schlafly, E. F., Smartt, S. J., Sweeney, W., Wainscoat, R. J., Burgett, W. S., Chastel, S., Grav, T., Heasley, J. N., Hodapp, K. W., Jedicke, R., Kaiser, N., Kudritzki, R. P., Luppino, G. A., Lupton, R. H., Monet, D. G., Morgan, J. S., Onaka, P. M., Shiao, B., Stubbs, C. W., Tonry, J. L., White, R., Bañados, E., Bell, E. F., Bender, R., Bernard, E. J., Boegner, M., Boffi, F., Botticella, M. T., Calamida, A., Casertano, S., Chen, W. P., Chen, X., Cole, S., Deacon, N., Frenk, C., Fitzsimmons, A., Gezari, S., Gibbs, V., Goessl, C., Goggia, T., Gourgue, R., Goldman, B., Grant, P., Grebel, E. K., Hambly, N. C., Hasinger, G., Heavens, A. F., Heckman, T. M., Henderson, R., Henning, T., Holman, M., Hopp, U., Ip, W. H., Isani, S., Jackson, M., Keyes, C. D., Koekemoer, A. M., Kotak, R., Le, D., Liska, D., Long, K. S., Lucey, J. R., Liu, M., Martin, N. F., Masci, G., McLean, B., Mindel, E., Misra, P., Morganson, E., Murphy, D. N. A., Obaika, A., Narayan, G., Nieto-Santisteban, M. A., Norberg, P., Peacock, J. A., Pier, E. A., Postman, M., Primak, N., Rae, C., Rai, A., Riess, A., Riffeser, A., Rix, H. W., Röser, S., Russel, R., Rutz, L., Schilbach, E., Schultz, A. S. B., Scolnic, D., Strolger, L., Szalay, A., Seitz, S., Small, E., Smith, K. W., Soderblom, D. R., Taylor, P., Thomson, R., Taylor, A. N., Thakar, A. R., Thiel, J., Thilker, D., Unger, D., Urata, Y., Valenti, J., Wagner, J., Walder, T., Walter, F., Watters, S. P., Werner, S., Wood-Vasey, W. M., and Wyse, R. (2016). The Pan-STARRS1 Surveys. *arXiv e-prints*, page arXiv:1612.05560.

- Cohen, M., Wheaton, W. A., and Megeath, S. T. (2003). Spectral Irradiance Calibration in the Infrared. XIV. The Absolute Calibration of 2MASS. *Astronomical Journal*, 126(2):1090–1096.
- Craig, M., Crawford, S., Seifert, M., Robitaille, T., Sipőcz, B., Walawender, J., Vinícius, Z., Ninan, J. P., Droettboom, M., Youn, J., Tollerud, E., Bray, E., Walker, N., Janga, V. R., Stotts, C., Günther, H. M., Rol, E., Bach, Y. P., Bradley, L., Deil, C., Price-Whelan, A., Barbary, K., Horton, A., Schoenell, W., Heidt, N., Gasdia, F., Nelson, S., and Streicher, O. (2017). `astropy/ccdproc`: v1.3.0.post1.
- Harris, C. R., Millman, K. J., van der Walt, S. J., Gommers, R., Virtanen, P., Cournapeau, D., Wieser, E., Taylor, J., Berg, S., Smith, N. J., Kern, R., Picus, M., Hoyer, S., van Kerkwijk, M. H., Brett, M., Haldane, A., del Río, J. F., Wiebe, M., Peterson, P., Gérard-Marchant, P., Sheppard, K., Reddy, T., Weckesser, W., Abbasi, H., Gohlke, C., and Oliphant, T. E. (2020). Array programming with NumPy. *Nature*, 585(7825):357–362.
- Hunter, J. D. (2007). Matplotlib: A 2d graphics environment. *Computing in Science & Engineering*, 9(3):90–95.
- Jordi, K., Grebel, E. K., and Ammon, K. (2006). Empirical color transformations between sdss photometry and other photometric systems. *A&A*, 460(1):339–347.
- Karttunen, H., Donner, K. J., Kröger, P., Oja, H., and Poutanen, M. (2016). *Tähtitieteen perusteet*, volume 6.
- Kato, T. (2015). WZ Sge-type dwarf novae. *Publications of the Astronomical Society of Japan*, 67(6):108.

- Kostov, A. and Bonev, T. (2018). Transformation of Pan-STARRS1 gri to Stetson BVRI magnitudes. Photometry of small bodies observations. *Bulgarian Astronomical Journal*, 28:3.
- Neustroev, V., Knigge, C., and Zharikov, S. (2018). Systematic search for post period-minimum cataclysmic variables: A short review. *PoS, GOLDEN* 2017:034.
- Oke, J. B. and Gunn, J. E. (1983). Secondary standard stars for absolute spectrophotometry. *Astrophysical Journal*, 266:713–717.
- Palmer, J. and Davenhall, A. C. (2001). The CCD Photometric Calibration Cookbook. *Starlink Cookbook*, 6.
- Price-Whelan, A. M., Sipőcz, B. M., Günther, H. M., Lim, P. L., Crawford, S. M., Conseil, S., Shupe, D. L., Craig, M. W., Dencheva, N., and et al. (2018). The astropy project: Building an open-science project and status of the v2.0 core package. *The Astronomical Journal*, 156(3):123.
- Skrutskie, M. F., Cutri, R. M., Stiening, R., Weinberg, M. D., Schneider, S., Carpenter, J. M., Beichman, C., Capps, R., Chester, T., Elias, J., Huchra, J., Liebert, J., Lonsdale, C., Monet, D. G., Price, S., Seitzer, P., Jarrett, T., Kirkpatrick, J. D., Gizis, J. E., Howard, E., Evans, T., Fowler, J., Fullmer, L., Hurt, R., Light, R., Kopan, E. L., Marsh, K. A., McCallon, H. L., Tam, R., Van Dyk, S., and Wheelock, S. (2006). The Two Micron All Sky Survey (2MASS). *Astronomical Journal*, 131(2):1163–1183.
- Smith, J., Tucker, D., Kent, S., Richmond, M., Fukugita, M., Ichikawa, T., Ichikawa, S.-I., Jorgensen, A., Uomoto, A., Gunn, J., Hamabe, M., Watanabe, M., Tolea, A., Henden, A., Annis, J., Pier, J., McKay, T., Brinkmann, J.,

Chen, B., Holtzman, J., Shimasaku, K., and York, D. (2002). The u'g'r'i'z' standard-star system. *Astronomical Journal*, 123(4 1756):2121–2144.

The Astropy Collaboration, Robitaille, Thomas P., Tollerud, Erik J., Greenfield, Perry, Droettboom, Michael, Bray, Erik, Aldcroft, Tom, Davis, Matt, Ginsburg, Adam, Price-Whelan, Adrian M., Kerzendorf, Wolfgang E., Conley, Alexander, Crighton, Neil, Barbary, Kyle, Muna, Demitri, Ferguson, Henry, Grollier, Frédéric, Parikh, Madhura M., Nair, Prasanth H., Günther, Hans M., Deil, Christoph, Woillez, Julien, Conseil, Simon, Kramer, Roban, Turner, James E. H., Singer, Leo, Fox, Ryan, Weaver, Benjamin A., Zabalza, Victor, Edwards, Zachary I., Azalee Bostroem, K., Burke, D. J., Casey, Andrew R., Crawford, Steven M., Dencheva, Nadia, Ely, Justin, Jenness, Tim, Labrie, Kathleen, Lim, Pey Lian, Pierfederici, Francesco, Pontzen, Andrew, Ptak, Andy, Refsdal, Brian, Servillat, Mathieu, and Streicher, Ole (2013). Astropy: A community python package for astronomy. *A&A*, 558:A33.

Tonry, J., Stubbs, C., Lykke, K., Doherty, P., Shivvers, I., Burgett, W., Chambers, K., Hodapp, K., Kaiser, N., Kudritzki, R.-P., Magnier, E., Morgan, J., Price, P., and Wainscoat, R. (2012). The pan-starrs1 photometric system. *Astrophysical Journal*, 750(2).

Warner, B. (1995). *Cataclysmic Variable Stars*. Cambridge Astrophysics. Cambridge University Press.